# Evidence for proton excitations in $^{130,132,134,136}$Xe isotopes from measurements of $g$ factors of $2_1^+$ and $4_1^+$ states

G. Jakob,[1] N. Benczer-Koller,[1] G. Kumbartzki,[1] J. Holden,[1] T. J. Mertzimekis,[1] K.-H. Speidel,[2] R. Ernst,[2] A. E. Stuchbery,[3] A. Pakou,[4] P. Maier-Komor,[5] A. Macchiavelli,[6] M. McMahan,[6] L. Phair,[6] and I. Y. Lee[6]

[1]*Department of Physics and Astronomy, Rutgers University, New Brunswick, New Jersey 08903*

[2]*Institut für Strahlen- und Kernphysik, Universität Bonn, Bonn, Germany*

[3]*Department of Nuclear Physics, Research School of Physical Sciences and Engineering, Australian National University, Canberra ACT 0200, Australia*

[4]*The University of Ioannina, 45110 Ioannina, Greece*

[5]*Physik-Department der Technischen Universität München, Munich, Germany*

[6]*Lawrence Berkeley National Laboratory, Berkeley, California 94720*

(Received 2 October 2001; published 22 January 2002)

The $g$ factors of $2_1^+$, $4_1^+$, and $2_2^+$ states in the stable $^{130,132,134,136}$Xe isotopes have been measured via projectile Coulomb excitation in inverse kinematics in combination with the transient field technique. The results show a steady decrease in $g(2_1^+)$ as the number of neutron holes increases in the lighter nuclei below the closed $N=82$ neutron shell. The $g$ factors of the $4_1^+$ states in $^{132,134}$Xe are consistently larger than the $g$ factors of the $2_1^+$ states, a characteristic of proton excitation. The $g$ factors of the $2_1^+$, $4_1^+$, and $2_2^+$ states in $^{130}$Xe are approximately equal as would be expected for vibrational excitations.

DOI: 10.1103/PhysRevC.65.024316 PACS number(s): 21.10.Ky, 25.70.De, 27.60.+j

## I. INTRODUCTION

The region $54<N<80$, spanning the isotopes of Ru, Pd, Cd, Ba, Xe, and Te, contains nuclei described by configurations lying between spherical and deformed $\gamma$-soft vibrators. This interpretation arises primarily from examination of the energies of excited states as well as transition probabilities. The ratios $R=E(4_1^+)/E(2_1^+)$ remain fairly stable between 2.0 and 2.5 for $62<N<80$, and the $B(E2)$'s decrease from about 80 to 20 Weisskopf units over the same interval. Even within the large statistical errors of the early experiments [1], the $g$ factors of the $2_1^+$ states conflict with the traditional interpretation, lying well below the value $Z/A$ expected for a collective vibrational state. This general trend is usually attributed to differences in pairing strengths for protons and neutrons [2]. However, in the case of the Xe isotopes and other nominally vibrational nuclei in transitional regions near closed shells, the effect of pairing may be less important because single particles can play a key role in the $g$ factors.

The advent of the interacting boson model, especially the version where neutrons and protons are treated separately [3,4], IBM-II, yielded remarkable agreement with the new, much more precise, $g$ factors of $2_1^+$ states of even-even nuclei from Ru to Te [5], obtained with the transient field technique [6,7]. The $B(E2;2_1^+\rightarrow 0_1^+)$'s calculated in this model, with constant effective charge for the entire isotopic chain, were in very good agreement with the experimental data [8]. A recent calculation of the $g$ factors of the $2_1^+$ states of Xe and Ba isotopes [9] with the wave functions of Ref. [8] and boson $g$ factors, $g_\pi=1$ and $g_\nu$ becoming increasingly more negative with increasing $A$, yielded results slightly smaller than the lowest-order IBA-II prediction: namely, $g=g_\pi(N_\pi/(N_\pi+N_\nu))+g_\nu(N_\nu/(N_\pi+N_\nu))$, where $g_\pi=1$ and $g_\nu=0$. The IBA-II model also predicted that the $g$ factors of $4_1^+$ states are equal to those of the $2_1^+$ states.

The success of IBM-II extended to heavier nuclei in the $88<N<120$ region. However, as in the lighter nuclei, major discrepancies between theoretical predictions and experiment arose when a new generation of very precise measurements of $g$ factors [10–12] became available. In the Nd and Sm isotopes, deviations from the model occurred not only as a function of $N$, but also as a function of spin [11,12]. These deviations were understood in terms of an important interplay of single-particle configurations with the emerging collective structure.

The stable even $^{124-136}$Xe isotopes, with four protons above the $Z=50$ shell closure and spanning the range from 70 neutrons to the closed shell at $N=82$, provide fertile ground to probe the development of collective structures as the number of neutron holes increases. Single-particle effects can be expected to dominate near the $N=82$ shell closure and may lead to variations in the $g$ factors of the low-excitation states. As the nuclei become collective, $g$ factor variations may still occur [13–15], but they are harder to explain in collective models, which, to first order, predict that all low-lying excited states have identical $g$ factors. $F$-spin-mixing mechanisms in the proton-neutron interacting boson model can account for $g(2_2^+)/g(2_1^+)$ variations of the order of $\leqslant 10\%$ [15,16], but differences between $g(2_1^+)$ and $g(4_1^+)$ require a mechanism outside the IBM-II model.

These considerations provided the motivation to measure the $g$ factors of the first $2^+$ and $4^+$ states of these Xe isotopes. The $g(4_1^+)$ factor of $^{136}$Xe [17] and the $g(2_1^+)$ factors of $^{124-132}$Xe [18–20] have been previously determined with the IMPAC and IPAC methods. However, these results depend directly on knowledge of the lifetimes of the nuclear states. Conventional transient field measurements of the $g(2_1^+)$ factors of $^{132,134,136}$Xe had been carried out using Xe-implanted carbon targets and iron as the ferromagnetic host [21]. In the current experiment, $g$ factors of $2_1^+$, $4_1^+$, and $2_2^+$

 

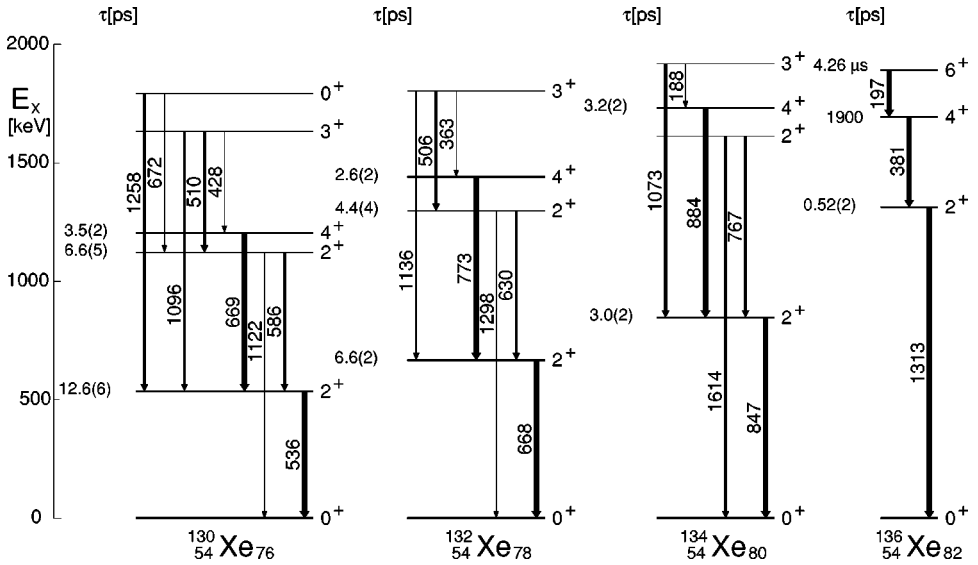


FIG. 1. Low-lying level schemes of the stable $^{130,132,134,136}$Xe isotopes [22–25]. The lifetimes indicated in the figure have been measured in the present experiment by the Doppler-shift attenuation method (DSAM) except those for the long-lived $4_1^+$ and $6_1^+$ states in $^{136}$Xe [25].

states in $^{130,132,134,136}$Xe isotopes were measured with the relatively high precision that ensues from inverse kinematics experiments carried out on beams. In addition, the high recoil velocity of the isotopes studied allowed measurements of mean lifetimes of various excited states by the Doppler-shift attenuation method (DSAM) with higher precision than quoted in the literature [22–25]. Figure 1 displays the low-lying energy levels of the stable $^{130,132,134,136}$Xe isotopes and Table I presents the available spectroscopic information.

## II. EXPERIMENTAL PROCEDURE AND DATA ANALYSIS

The experimental procedure and subsequent analysis of the data follow very closely the recent work on Kr isotopes [26]. In the present work, isotopically pure $^{130,132,134,136}$Xe beams with energies between 485 and 508 MeV were provided by the 88-Inch Cyclotron at the Lawrence Berkeley National Laboratory. A multilayered target was used, consisting of a 1.0 mg/cm$^2$ $^{nat}$Ti excitation layer, onto which 5.2 mg/cm$^2$ of gadolinium was evaporated at high temperature [27]. A copper stopper layer of 4.9 mg/cm$^2$ on the backside of the gadolinium provided good thermal conductivity. An additional 9.0 mg/cm$^2$ copper foil was placed behind the target as a beam stop.

The $^{130,132,134,136}$Xe projectiles were Coulomb excited to their $2_1^+$, $4_1^+$, and $2_2^+$ states by impinging on the $^{nat}$Ti target layer and subsequently traversed the polarized ferromagnetic gadolinium layer, where they experienced spin precession in the transient magnetic hyperfine field. The excited Xe ions

TABLE I. Spectroscopic data on the low-lying levels of $^{130,132,134,136}$Xe [22–25]. Energies are in MeV, mean lifetimes $\tau$ in ps, $B(E2)$'s in Weisskopf units, and $B(M1)$'s in $\mu_N^2$. The first line of the lifetime and $B(E2)$ data presents the results from the DSAM analysis of the current experiment, while the data marked by an asterisk (*) are from Refs. [22–25].

| | $^{130}_{54}$Xe$_{76}$ | $^{132}_{54}$Xe$_{78}$ | $^{134}_{54}$Xe$_{80}$ | $^{136}_{54}$Xe$_{82}$ |
|---|---|---|---|---|
| $E(2_1^+)$ | 0.5361 | 0.6677 | 0.8470 | 1.3130 |
| $\tau(2_1^+)$ | 12.6(6) | 6.6(2) | 3.0(2) | 0.52(2) |
| | 12.4(14)* | 6.8(3)* | 2.7(6)* | 0.59(26)* |
| $E(2_2^+)$ | 1.1221 | 1.2979 | 1.6138 | 2.2895 |
| $\tau(2_2^+)$ | 6.6(5) | 4.4(4) | — | — |
| $E(4_1^+)$ | 1.2046 | 1.4403 | 1.7312 | 1.6944 |
| $\tau(4_1^+)$ | 3.5(2) | 2.6(2) | 3.2(2) | $1.90\cdot10^3$* |
| $E(4_1^+)/E(2_1^+)$ | 2.247 | 2.157 | 2.044 | 1.290 |
| $I(2_2^+\rightarrow2_1^+)/I(2_2^+\rightarrow0_1^+)$ | 6.49(29) | 14.9(14) | 0.96(6) | 0.26(2) |
| $\delta(2_2^+\rightarrow2_1^+)$ | +3.75(12) | +4.07(16) | −2.4(2) | — |
| $B(E2;\ 2_1^+\rightarrow0_1^+)$ | 37.1(17) | 23.7(6) | 14.7(1) | 10.3(4) |
| | 38(5)* | 23.2(10)* | 17.7(33)* | 9.0(40)* |
| $B(E2;\ 4_1^+\rightarrow2_1^+)$ | 44.5(20) | 28.8(24) | 12.1(8) | 1.25(6)* |
| $B(E2;\ 2_2^+\rightarrow2_1^+)$ | 37.1(28) | 41.3(33) | — | — |
| $B(M1;\ 2_2^+\rightarrow2_1^+)$ | 0.00247(23) | 0.00276(30) | — | — |
| $B(E2;\ 2_2^+\rightarrow0_1^+)$ | 0.238(20) | 0.079(9) | — | — |

TABLE II. Characteristics of the reaction kinematics. Energies are given in MeV. $\langle E\rangle_{in}$, $\langle E\rangle_{out}$, $\langle v/v_0\rangle_{in}$, and $\langle v/v_0\rangle_{out}$ are the calculated average energies and velocities of the excited Xe ions as they enter into and exit from the gadolinium target layer. $v_0 = e^2/\hbar$ is the Bohr velocity.

| Isotope | $E_{beam}$ | $\langle E\rangle_{in}$ | $\langle E\rangle_{out}$ | $\langle v/v_0\rangle_{in}$ | $\langle v/v_0\rangle_{out}$ |
|---|---|---|---|---|---|
| $^{130}$Xe | 509 | 111.7 | 12.8 | 5.89 | 1.99 |
| $^{132}$Xe | 499 | 111.4 | 13.1 | 5.83 | 2.00 |
| $^{134}$Xe | 492 | 111.8 | 13.7 | 5.80 | 2.03 |
| $^{136}$Xe | 485 | 112.2 | 14.3 | 5.77 | 2.06 |

come to rest and decay in the copper target layer, free from further hyperfine interactions. The kinematics of the excited Xe ions, calculated from the stopping powers tabulated by Ziegler *et al.* [28], are summarized in Table II.

The recoiling titanium ions passed through the target and copper foil and were detected in a rectangular solar cell detector. This particle detector, centered at 0° relative to the beam, subtended angular ranges of ±25° perpendicular to and ±11° parallel to the $\gamma$ detection plane. The shape of the particle detector was chosen to enhance the angular correlation [29]. In order to provide good ferromagnetic properties for the gadolinium layer throughout the spin precession measurements, the target was mounted on the tip of a magnet which was cooled by liquid nitrogen. The magnetization of the target was measured before and after the experiment in an ac magnetometer [30] and found to remain constant at $M=0.1613$ T. Two iron cones span the space between the target and the input collimator on the upstream side and the particle detector on the downstream side to eliminate possible bending of the beam and recoiling ions in the stray external magnetic field applied to align the magnetization of the gadolinium foil. Deexcitation $\gamma$ rays were detected in two pairs of Ge detectors with relative efficiencies of 40% and 50%, respectively, located upstream and downstream of the target. In addition, a 25% Ge detector was placed at 0°. Figure 2 shows the coincidence spectra observed for the $^{130,132,134,136}$Xe isotopes. The observed transition intensities, corrected for their angular correlations, were in excellent agreement with Coulomb excitation calculations [31].

The major advantage of the inverse reaction kinematics over the standard reaction is that several isotopes can be measured with the same target. This feature diminishes systematic errors attributed to uncertainties in the layer thicknesses and ferromagnetic properties of the delicate multilayered targets. Another important advantage arises from the kinematic focusing of the coincident lighter target ions detected by the particle detector at 0°, which provides a much higher excitation yield for the states of interest.

### A. Determination of the precession angle $\Delta\theta$

The precession angle of the excited nuclear state is determined as the ratio of the spin precession "effect" $\epsilon$ and the logarithmic slope of the angular correlation, $S = (1/W)dW/d\theta$:

$$\Delta\theta = \epsilon/S.$$

These two quantities are measured separately.

The particle-$\gamma$ angular correlations $W(\theta_\gamma)$ were determined from anisotropy measurements in which the $\gamma$ detectors were alternately placed at angles ±50°, ±130° and ±80°, ±100°. Anisotropy ratios were thereby independently derived from the two detector pairs and are given by the cross ratios

$$R(130°/100°) = \sqrt{\frac{N_1(-130°)}{N_1(-100°)}\,\frac{N_4(+130°)}{N_4(+100°)}}$$

and

$$R(50°/80°) = \sqrt{\frac{N_2(-50°)}{N_2(-80°)}\,\frac{N_3(+50°)}{N_3(+80°)}},$$

where $N_i(\theta_\gamma)$ are the coincidence counting rates of the photopeak of the $\gamma$ transition in the $i$th detector and are proportional to $W_i(\theta_\gamma)$.

By constructing the ratios in this way, many systematic errors cancel, including uncertainties in the beam current, time of measurement, and relative efficiencies of the detectors. $W(\theta_\gamma)$ was extracted from these ratios, and the logarithmic slope was calculated at the detector position in the "effect" measurement as described in [26].

To measure the "effect" $\epsilon$, an external magnetic field of $B_{ext}=0.06$ T was applied alternately ↑ ("up") and ↓ ("down") with respect to the $\gamma$-ray detection plane. The four Ge detectors were placed at ±66° and ±114° with respect to the beam axis. $\epsilon$ is then expressed as the ratio

$$\epsilon = \frac{\rho-1}{\rho+1},$$

where the "double ratio" $\rho=\sqrt{\rho_{1,4}/\rho_{2,3}}$ is constructed from ratios of coincidence counting rates of the two pairs of detectors:

$$\rho_{i,j} = \sqrt{\frac{N_i^{\uparrow}\cdot N_j^{\downarrow}}{N_i^{\downarrow}\cdot N_j^{\uparrow}}}.$$

As in the case of the anisotropy ratios, the ratios $\rho$ are designed such that most systematic errors cancel.

This analysis was sufficient to determine the $g$ factors of the $2_1^+$ states in $^{134,136}$Xe, which are not appreciably fed by higher states. However, the analysis of the $2_1^+$ states in $^{130,132}$Xe is more complex due to considerable feeding contributions from the $2_2^+$ and $4_2^+$ states. In these cases, the observed decays of the $2_1^+$ states contain contributions from the higher states which must be subtracted in order to obtain $\epsilon$ and $S$ corresponding to the precession of the magnetic moment of the state of interest. The details of the analysis were presented in [15,26,32].

### B. Measurement of lifetimes

Mean lifetimes of $2_1^+$ and $4_1^+$ states in $^{130,132,134,136}$Xe isotopes were determined from the DSAM analysis [33] of

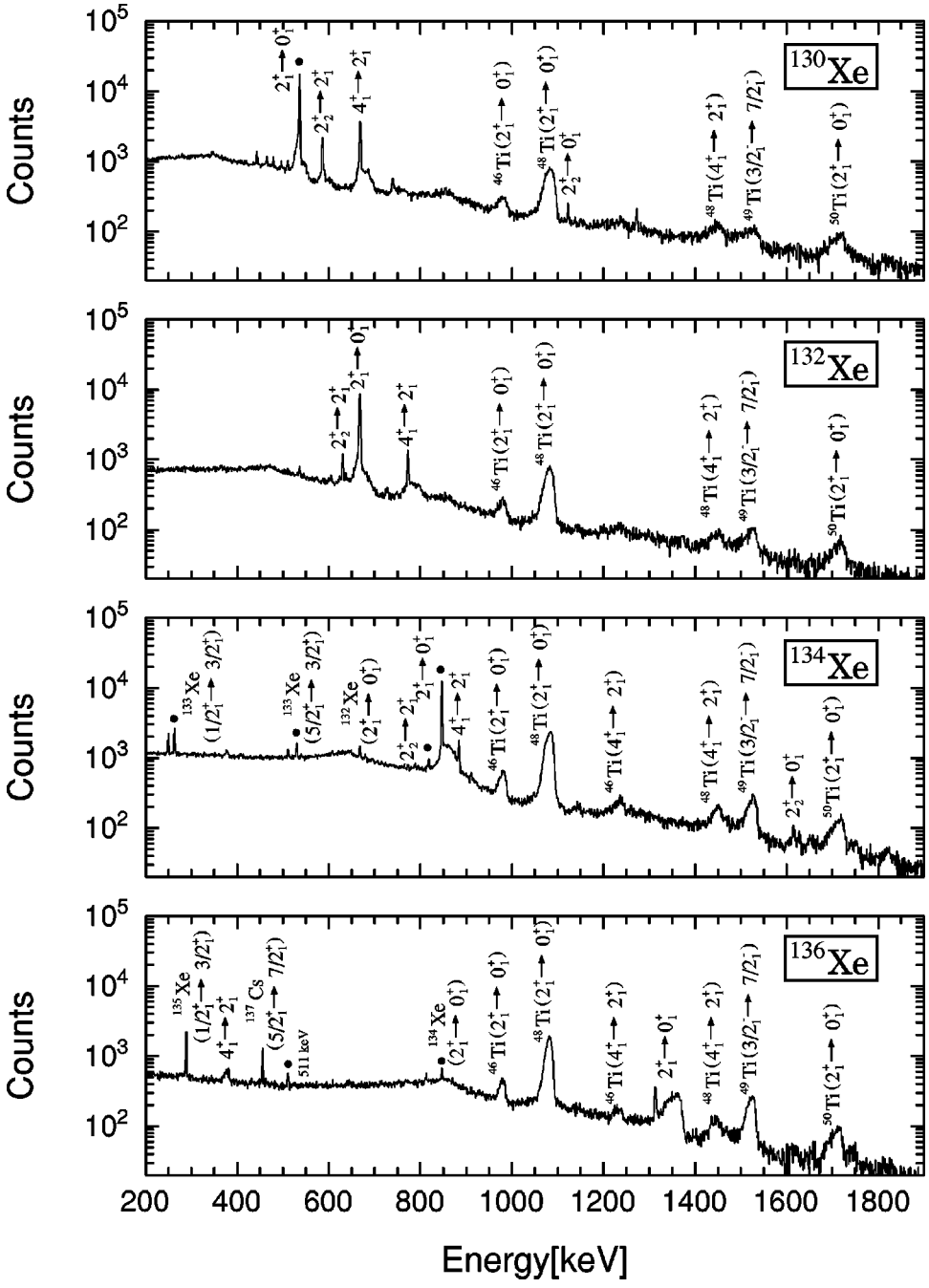


FIG. 2. Particle-$\gamma$ coincidence spectra for $^{130,132,134,136}$Xe taken with the Ge detector placed at 0° with respect to the beam axis. Most $\gamma$ transitions result from the Xe projectile and Ti target Coulomb excitation. Additional transitions attributed to excited levels of neighboring isotopes, which were produced via neutron transfer reactions, were observed. Several of the most intense ones are marked. The peaks marked by dots are described by the adjacent labels.

the Doppler-broadened line shapes observed in detectors located at 0°, 50°, and 66° with respect to the beam. In each case, the best spectra were chosen on the basis of achieving a balance between statistics and higher resolution of shifted and stopped contributions to the peaks. Side feeding contributions to the $2_1^+$ state from the $4_1^+$ state decay were taken into account.

Figure 3 displays the DSAM fits to the Doppler-broadened lineshapes of the $4_1^+ \rightarrow 2_1^+$ transitions in $^{130,132,134}$Xe and of the $2_1^+ \rightarrow 0_1^+$ transition in $^{136}$Xe. Lifetimes of the $4_1^+$ states of $^{130,132,134}$Xe and $2_2^+$ states of $^{130,132}$Xe have been measured for the first time. The mean lifetimes of the $2_1^+$ states obtained in this experiment (Table I) are in agreement with the results of previous measurements [22–25]. The stopping powers of Ref. [28] were used in the analysis. The quoted errors were obtained by doubling the statistical errors in the measurement to account for possible systematic uncertainties in the DSAM arising from the complex nature of the target.

## III. RESULTS

The $g$ factors were deduced from the measured precession angles $\Delta\theta = \epsilon/S$ by the expression

$$\Delta\theta = -g\frac{\mu_N}{\hbar}\int_{t_{in}}^{t_{out}} B_{TF}(v(t),Z)e^{-t/\tau}\,dt, \qquad (1)$$

where $B_{TF}$ is the transient field, which depends on the veloc-

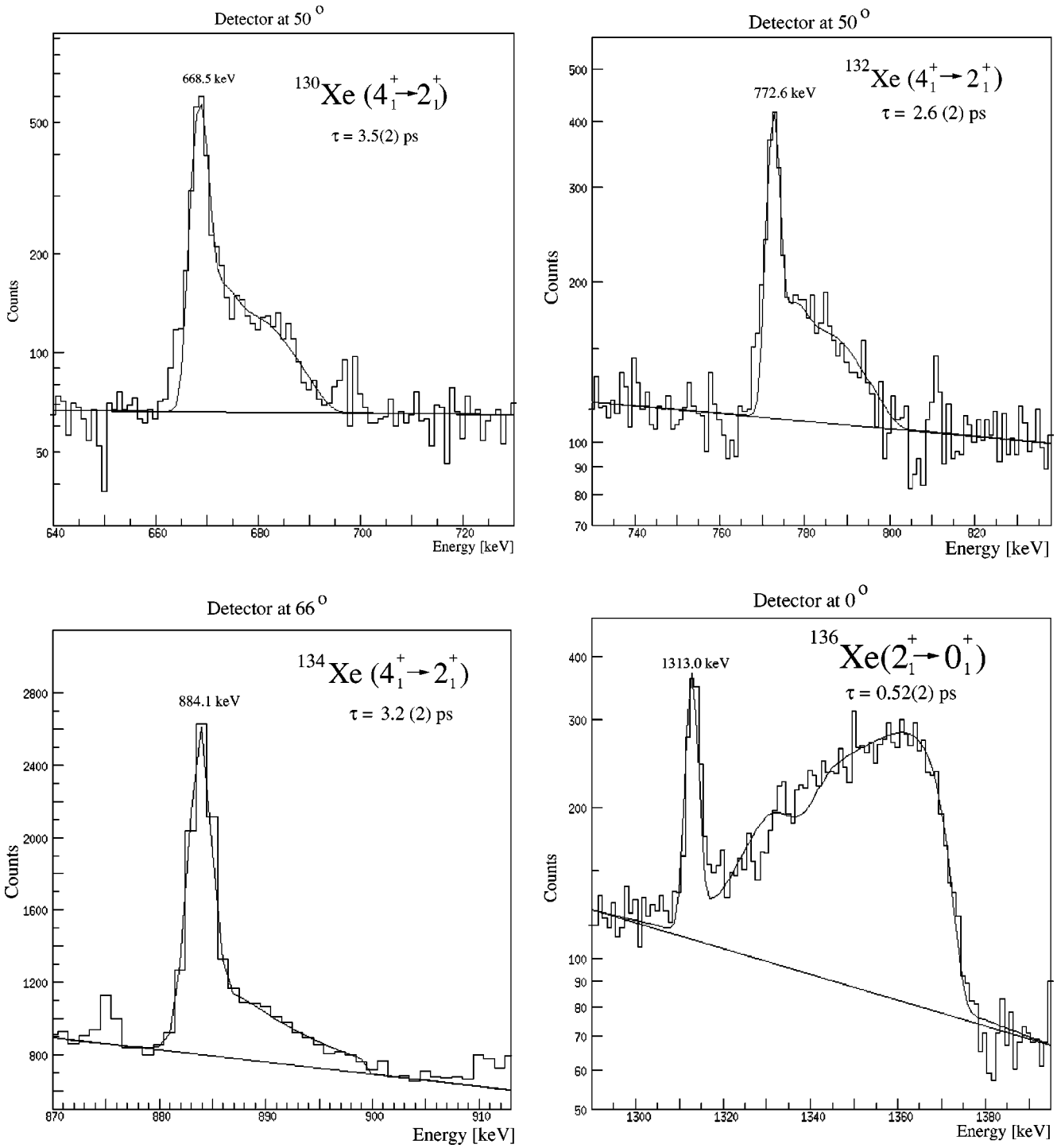


FIG. 3. DSAM analysis of the $4_1^+ \rightarrow 2_1^+$ transitions in the $^{130,132,134}$Xe even isotopes and the $2_1^+ \rightarrow 0_1^+$ transition in $^{136}$Xe. The solid line represents the best fit to the data. The wiggle in the fitted line, which is very pronounced for the $^{136}$Xe $2_1^+ \rightarrow 0_1^+$ transition, arises from the layered structure of the target. Most of the intensity under the stopped peak corresponds to feeding from the decay of the long-lived $4_1^+$ state.

ity $v$ and atomic number $Z$ of the probe ion, $\tau$ is the mean lifetime of the state being examined, and $t_{in}$ and $t_{out}$ are the mean entrance and exit times of the ions traversing the gadolinium layer. The Rutgers parametrization [7] was used to evaluate the strength of the transient field. The slopes, precession angles, and resulting $g$ factors are summarized in Table III. The precession of the magnetic moment of the long-lived $4_1^+$ state in $^{136}$Xe was corrected for the precession in the 0.06 T external magnetic field. Table IV compares the results of this experiment with the data from previous measurements.

As can be seen from Table IV, the $g(2_1^+)$ factors of the $^{130,132,134,136}$Xe isotopes are in qualitative agreement with previous IMPAC and transient field measurements which had

TABLE III. Results of the measurements of the logarithmic slopes $S(\theta_\gamma)$ of the particle-$\gamma$ angular correlation of the individual nuclear states, the spin precession angles $\Delta\theta$, and the $g$ factors.

| | $\lvert S(66°)\rvert$ | $\Delta\theta$ (mrad) | $g$ | $\lvert S(66°)\rvert$ | $\Delta\theta$ (mrad) | $g$ | $\lvert S(66°)\rvert$ | $\Delta\theta$ (mrad) | $g$ |
|---|---|---|---|---|---|---|---|---|---|
| | | $2_1^+$ | | | $4_1^+$ | | | $2_2^+$ | |
| $^{130}_{54}Xe_{76}$ | 2.495(23) | −30.7(10) | +0.334(11) | 0.943(7) | −34.8(43) | +0.42(5) | 0.724(7) | −38.8(77) | +0.45(9) |
| $^{132}_{54}Xe_{78}$ | 2.553(27) | −26.9(10) | +0.314(12) | 0.961(9) | −46.9(85) | +0.61(11) | 0.710(8) | −6.8(178) | +0.1(2) |
| $^{134}_{54}Xe_{80}$ | 2.595(14) | −27.7(5) | +0.354(7) | 0.972(5) | −62.3(117) | +0.80(15) | — | — | — |
| $^{136}_{54}Xe_{82}$ | 2.675(41) | −30.4(16) | +0.766(45) | 0.989(9) | −104.7(420) | +1.08(43)[a] | — | — | — |

[a]The observed effect for this long-lived state has been corrected for the precession in the external field.

been carried out under different experimental conditions. The average of the IMPAC $g(2_1^+)$ factor measurements, of previous transient field data and the new results for the $g(4_1^+)$ and $g(2_2^+)$ factors, are shown in Fig. 4. The $g$ factors of the $4_1^+$ states of the $^{130,132,134}$Xe isotopes have been measured for the first time. The $g$ factor of the $4_1^+$ state in $^{136}$Xe was measured previously in a radioactivity measurement [17].

## IV. DISCUSSION

The $g(2_1^+)$ data displayed in Fig. 4 lie well below $Z/A$, the prediction of collective models. As expected, the $g$ factors of the $2_1^+$ and $4_1^+$ states in $^{136}$Xe are large, supporting proton excitations. As a first approximation both states are expected to be described by a $g_{7/2}$ proton configuration. A recent calculation within the framework of cranked Hartree-Fock-Bogoliubov formalism [34] predicts $g(2_1^+;{}^{136}\mathrm{Xe}) = 1.0022$, somewhat larger than the experimental results, and $g(4_1^+;{}^{136}\mathrm{Xe}) = 0.8227$, in good agreement with the data. The calculations also agree with the data for $g(2_1^+)$ and $g(6_1^+)$ in $^{138}$Ba, but overpredict $g(4_1^+)$.

The $g(2_1^+)$ of the lighter isotopes decrease steadily as the number of neutron holes in the closed $N=82$ shell is increased, as expected since the $h_{11/2}$ neutron configuration, with its negative $g$ factor, should play an increasing role. On the other hand, the behavior of $g(4_1^+)$ differs from that of $g(2_1^+)$. It is probably a coincidence that $g(4_1^+)$ follows the IBA prediction since these $g$ factors are more realistically interpreted as evidence for proton excitations near $N=82$.

The value of $g(^{132}\mathrm{Xe};\ 2_2^+)$ tends to be small, suggesting a configuration dominated by neutron single-particle states. Interestingly, the $g$ factors of the $2_1^+$, $4_1^+$, and $2_2^+$ states of $^{130}$Xe have the same value within errors, in agreement with the collective picture where $g=Z/A$.

The $N=82$ isotones near $Z=50$ have been the subject of a number of recent shell model studies in which the valence proton configurations were unrestricted within the 50–82 major shell and different residual interactions were employed [36–38]. The semimagic Sn isotopes have also been studied recently by shell model calculations in which the valence neutron configuration was unrestricted within the 50–82 neutron shell, and realistic two-body residual interactions were employed [39].

To date, the calculations have emphasized level energies and sometimes transition rates. Theoretical work which calculates the magnetic moments in nuclei near $N=82$ is scant.

TABLE IV. Comparison of previous measurements of $g(2_1^+)$ and $g(4_1^+)$ with the current data. The data of Ref. [21] were reanalyzed with the newly determined lifetimes and the linear parametrization of the transient field in iron determined in Ref. [35].

| $2_1^+$ | Ref. [18] | Ref. [19] | Ref. [20] | Ref. [21] | This work |
|---|---|---|---|---|---|
| $^{124}_{54}Xe_{70}$ | | +0.23(2) | | | |
| $^{126}_{54}Xe_{72}$ | | +0.27(4) | +0.37(7) | | |
| $^{128}_{54}Xe_{74}$ | | +0.31(3) | +0.41(7) | | |
| $^{130}_{54}Xe_{76}$ | | +0.31(4) | +0.38(7) | | +0.334(11) |
| $^{132}_{54}Xe_{78}$ | +0.38(6) | +0.39(5) | +0.37(5) | +0.349(34) | +0.314(12) |
| $^{134}_{54}Xe_{80}$ | | | | +0.504(49) | +0.354(7) |
| $^{136}_{54}Xe_{82}$ | | | | +0.83(10) | +0.766(45) |
| $4_1^+$ | Ref. [17] | | | | This work |
| $^{136}_{54}Xe_{82}$ | +0.80(15) | | | | +1.08(43) |

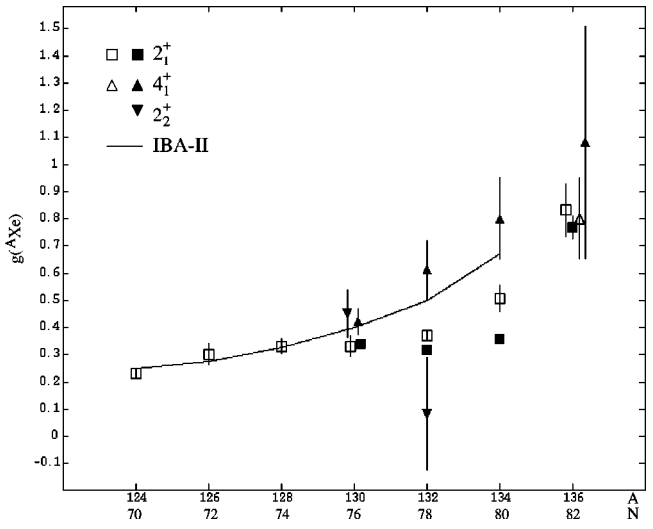


FIG. 4. Comparison of the $g$ factors measured in this experiment (solid symbols) with the average of previous data (open symbols) in Refs. [17–21]. The solid line represents the IBA-II model prediction, $g=g_\pi(N_\pi/(N_\pi+N_\nu))+g_\nu(N_\nu/(N_\pi+N_\nu))$ (with $g_\pi=1$ and $g_\nu=0$).

TABLE V. Single-particle energies and calculated $g$ factors for proton and neutron-hole orbits in $^{131}_{50}Sn_{81}$ and $^{133}_{51}Sb_{82}$. The effective orbital and spin $g$ factors are discussed in the text.

| Orbit | Neutron holes: $^{131}_{50}Sn_{81}$ | | Protons: $^{133}_{51}Sb_{82}$ | |
|---|---|---|---|---|
| | $E_x$ (keV) | $g$ | $E_x$ (keV) | $g$ |
| $2d_{3/2}$ | 0 | +0.554 | 2439 | +0.544 |
| $1h_{11/2}$ | 242 | −0.223 | 2793 | +1.39 |
| $3s_{1/2}$ | 332 | −2.65 | 2920 | +4.04 |
| $2d_{5/2}$ | 1655 | −0.514 | 962 | +1.54 |
| $1g_{7/2}$ | 2434 | +0.317 | 0 | +0.803 |

An exception is the work of White *et al.* [40], wherein the moments of the $7/2^+$ ground states in the odd-$A$, $N=82$, isotones have been studied in some detail, along with the $7/2^+$ ground states of the $N<82$ isotopes of Sb. Recently, magnetic moments have been calculated with different shell model calculations in a few cases in neutron-rich nuclei near $^{132}_{50}Sn$ [41].

A new set of shell model calculations (OXBASH [42]) has been performed for the Xe and Te isotopes near $N=82$ where the valence protons occupied the $Z=50$–$82$ shell and the neutron (holes) were in the $N=50$–$82$ shell. In other words, valence protons and neutrons were added to a $^{100}_{50}Sn_{50}$ core. The single-particle energies were chosen to reproduce the single-proton states in $^{133}_{51}Sb_{82}$ and the single-neutron-hole states in $^{131}_{50}Sn_{81}$ (Table V). Surface delta interactions (SDIs) were used to represent the two-body residual interactions. The proton-proton ($A_{\pi\pi}=0.23$MeV) and neutron-neutron ($A_{\nu\nu}=0.19$ MeV) interactions give comparable descriptions of the level energies in $^{134}_{52}Te_{82}$ and $^{130}_{50}Sn_{80}$, respectively. The calculated spectrum of $^{132}_{51}Sb_{81}$ is not very sensitive to the strength of the SDIs. The value $A_{\pi\nu}=0.25$ MeV was adopted, based on the expectation that $A_{\pi\nu}\sim A_{\pi\pi}\sim A_{\nu\nu}\sim 25/A$ MeV, and that this value gave a slightly better description of $^{132}_{51}Sb_{81}$ than the lower values adopted for the proton-proton and neutron-neutron interactions.

Since core polarization and meson-exchange currents affect the single-particle $g$ factors, the orbital and spin $g$ factors of the neutron were chosen to give a good account of the experimental $g$ factors of the $(3/2)^+$ $(2d_{3/2})$ and $11/2^-$ $(1h_{11/2})$ states in $^{135}_{54}Xe_{81}$. The corresponding quantities for the proton were chosen to reproduce the $g$ factors of the low-lying $(7/2)^+(1g_{7/2})$ and $(5/2)^+(2d_{5/2})$ states in the odd-$Z$, $N=82$ isotones [1]. The values adopted are $g_l(\pi)=1.13$, $g_s(\pi)=4.04=0.72g_s^{free}(\pi)$, $g_l(\nu)=0.02$, and $g_s(\nu)=-2.65=0.69g_s^{free}(\nu)$. For the protons, the effective single-nucleon $g$ factors are close to those calculated in Ref. [40]. The single-proton and single-neutron-hole spectra are shown in Table V together with their single-particle $g$ factors.

The striking feature of the single-particle spectra shown in

TABLE VI. Calculated $g$ factors for the lowest states of spin 2, 4, and 6 in the even Te and Xe isotopes and comparison with experimental values. Calculation I considers a shell closed at $N,Z=64$, while calculation II utilizes the full 50–82 shell.

| | | $^{134}_{52}Te_{82}$ | $^{132}_{52}Te_{80}$ | $^{130}_{52}Te_{78}$ | $^{136}_{54}Xe_{82}$ | $^{134}_{54}Xe_{80}$ | $^{132}_{54}Xe_{78}$ |
|---|---|---|---|---|---|---|---|
| $2_1^+$ | Calc. I | +0.811 | +0.648 | +0.598 | +0.812 | +0.594 | +0.510 |
| | Calc. II | +0.858 | +0.448 | +0.445 | +0.861 | | |
| | Expt. | | | +0.297(35) [a] | +0.766(45) | +0.354(7) | +0.314(12) |
| $2_2^+$ | Calc. I | +0.736 | +0.399 | +0.229 | +0.812 | +0.463 | +0.423 |
| | Calc. II | +0.947 | +0.490 | +0.448 | +0.828 | | |
| | Expt. | | | | | | +0.1(2) |
| $4_1^+$ | Calc. I | +0.810 | +0.789 | +0.766 | +0.811 | +0.780 | +0.740 |
| | Calc. II | +0.823 | +0.804 | | +0.827 | | |
| | Expt. | | | | | +0.83(14) [b] | 0.61(11) |
| $4_2^+$ | Calc. I | +1.097 | −0.167 | −0.174 | +0.810 | +0.782 | +0.739 |
| | Calc. II | +1.146 | −0.154 | | +0.838 | | |
| $6_1^+$ | Calc. I | +0.816 | +0.804 | +0.786 | +0.818 | +0.800 | +0.777 |
| | Calc. II | +0.817 | +0.807 | | +0.823 | | |
| | Expt. | +0.846(25) [c] | +0.79(9) [d] | | | | |
| $6_2^+$ | Calc. I | +1.169 | −0.010 | −0.057 | +1.165 | +0.560 | +0.429 |
| | Calc. II | +1.168 | −0.112 | | +1.160 | | |

[a]Average of $g$ factors quoted in Ref. [1].
[b]Average of $g$ factors of Ref. [17] and present work.
[c]Reference [43].
[d]Reference [44].

Table V is the subshell gap between the $2d_{3/2}$, $1h_{11/2}$, and $3s_{1/2}$ orbits and the $2d_{5/2}$ orbit. It follows that the valence proton excitations in the even Xe isotopes will involve predominantly $\pi 1g_{7/2}$ configurations with some $\pi 2d_{5/2}$ admixtures and much weaker contributions from $\pi 2d_{3/2}$, $\pi 1h_{11/2}$, and $\pi 3s_{1/2}$. In contrast, the close proximity of the corresponding neutron-hole orbits near the Fermi surface, namely, $\nu 2d_{3/2}$, $\nu 1h_{11/2}$, and $\nu 3s_{1/2}$, implies that the low-lying low-spin neutron excitations will have mixed contributions from all three of these orbits. As a first approximation a set of calculations (Table VI) with closed $N=64$ and $Z=64$ subshells (calculation I) was run for the nuclei $^{130,132,134}_{52}$Te and $^{132,134,136}_{54}$Xe. Since the interactions were not adjusted to account for the truncated space, these give a relatively poor description of the excitation energies. However, these calculations do define the dominant components of the wave functions and hence give a first semiquantitative estimate of the $g$ factors. A second set of calculations (calculation II) with no restrictions on the valence configurations in the 50–82 major shell was also performed. As a result of limitations on the number of configurations that can be included in the calculation, this approach could only be used for $^{136}_{54}Xe_{82}$ and $^{132,134}_{52}Te_{80,82}$ and for the $2^+$ states in $^{130}_{52}Te_{78}$.

The calculations indicate that the proton excitations are mainly $\pi 2d_{5/2}$ while the neutron configurations are a mix of $\nu 2d_{3/2}$ and $\nu 1h_{11/2}$, with the $\nu 1h_{11/2}$ orbit being more dominant as the spin increases. The neutron $\nu 3s_{1/2}$ orbit plays a much smaller role.

For $N<82$, the $4^+$ states consistently have larger $g$ factors than the $2^+$ states, in agreement with experiment, and there is a tendency for the second $2^+$ state to have a smaller $g$ factor than the first $2^+$ state ($N<82$), but this trend can be quenched or even reversed if the basis space is increased.

As expected, increasing the size of the basis space usually pushes the low-excitation $g$ factors closer to the collective model values and suppresses the variations seen in the limited-basis calculations. The fact that the experimentally observed $g$-factor variations are quenched in the large basis calculations suggests that the residual interactions, and particularly the proton-neutron interactions, need refining.

It is interesting to note that the yrast states in Te and Xe behave similarly, but nonyrast states can have very different structures. For example, the sign reversals predicted for the $g$ factors of the $2_2^+$ and $4_2^+$ states in the $^{130,132}Te_{78,80}$ isotopes are not present in the corresponding Xe isotones.

From the point of view of the present calculations, it is very difficult to obtain a small value for $g(2_2^+)$ in $^{132}_{54}Xe_{82}$ because the two lowest $2^+$ states have similar structures and the larger basis calculations drive their calculated values toward $Z/A$. The immediate suggestion is that the proton-neutron interactions are too strong. The calculations also yield larger $g(2_1^+)$ than experiment. It is certainly possible to adjust the residual interactions to improve the calculations of the $2^+$ state energies and this aspect should be considered in future work. However, with even a few valence nucleons there are likely to be collective components in the lowest $2^+$ state that are not easily included in shell model calculations, and it may be necessary to employ a particle-core model [45] to describe the interplay of collective and single-particle features.

In summary, high-precision $g$-factor data were obtained for low-lying $2^+$ and $4^+$ states in $^{130,132,134,136}$Xe using a new experimental technique involving Coulomb excitation of beam projectiles in inverse kinematics combined with the transient field method. These precise experimental $g$ factors, examined in conjunction with level energies, transition probabilities, and a first set of shell model calculations, are able to provide detailed information on wave functions of these excited nuclei. A complex picture of single-particle interactions coupled to collective motions is required to explain the observed $g$-factor variations.

## ACKNOWLEDGMENTS

The authors are indebted to the staff of the 88-Inch Cyclotron of the Lawrence Berkeley National Laboratory for their assistance during the experiment. One of us (K.-H.S.) wishes to thank the Rutgers Nuclear Physics Laboratory for hosting summer visits during 1998–2000. A.E.S. acknowledges the support of the Australian Academy of Science International Exchange Program. The work was supported in part by the BMBF, the Deutsche Forschungsgemeinschaft, the U.S. National Science Foundation, and the U.S. Department of Energy under Grant No. DE-FG02-91ER-40609.

[1] P. Raghavan, At. Data Nucl. Data Tables **42**, 189 (1989).
[2] W. Greiner, Nucl. Phys. **80**, 417 (1966).
[3] M. Sambataro and A. E. L. Dieperink, Phys. Lett. **107B**, 249 (1981).
[4] M. Sambataro, O. Scholten, A. E. L. Dieperink, and G. Piccitto, Nucl. Phys. **A423**, 333 (1984).
[5] N. K. B. Shu, R. Levy, N. Tsoupas, A. Lopez-Garcia, W. Andrejtscheff, and N. Benczer-Koller, Phys. Rev. C **24**, 954 (1981).
[6] N. Benczer-Koller, M. Hass, and J. Sak, Annu. Rev. Nucl. Sci. **30**, 53 (1980).
[7] N. K. B. Shu, D. Melnik, J. M. Brennan, W. Semmler, and N. Benczer-Koller, Phys. Rev. C **21**, 1828 (1980).
[8] G. Puddu, O. Scholten, and T. Otsuka, Nucl. Phys. **A348**, 109 (1980).
[9] T. Otsuka, Hyperfine Interact. **78**, 19 (1993).
[10] K.-H. Speidel, N. Benczer-Koller, G. Kumbartzki, C. Barton, A. Gelberg, J. Holden, G. Jakob, N. Matt, R. H. Mayer, M. Satteson, R. Tanczyn, and L. Weissman, Phys. Rev. C **57**, 2181 (1998).
[11] J. Holden, N. Benczer-Koller, G. Jakob, G. Kumbartzki, T. J. Mertzimekis, K.-H. Speidel, A. Macchiavelli, M. McMahan, L. Phair, P. Maier-Komor, A. E. Stuchbery, W. F. Rogers, and A. D. Davies, Phys. Lett. B **493**, 7 (2000).
[12] J. Holden, N. Benczer-Koller, G. Jakob, G. Kumbartzki, T. J. Mertzimekis, K.-H. Speidel, C. W. Beausang, R. Krücken, A.

Macchiavelli, M. McMahan, L. Phair, A. E. Stuchbery, P. Maier-Komor, W. F. Rogers, and A. D. Davies, Phys. Rev. C **63**, 024315 (2001).
[13] T. Vass, A. W. Mountford, G. Kumbartzki, N. Benczer-Koller, and R. Tanczyn, Phys. Rev. C **48**, 2640 (1993), and references therein.
[14] N. Matt, N. Benczer-Koller, J. Holden, G. Kumbartzki, R. H. Mayer, M. Satteson, and R. Tanczyn, Phys. Rev. C **59**, 665 (1999), and references therein.
[15] A. E. Stuchbery, I. Morrison, L. D. Wood, R. A. Bark, H. Yamada, and H. H. Bolotin, Nucl. Phys. **A435**, 635 (1985).
[16] S. Kuyucak and A. E. Stuchbery, Phys. Lett. B **348**, 315 (1995).
[17] Z. Berant, A. Wolf, J. C. Hill, F. K. Wohn, R. L. Gill, H. Mach, M. Rafailovich, H. Kruse, B. H. Wildenthal, G. Peaslee, A. Aprahamian, J. Goulden, and C. Chung, Phys. Rev. C **31**, 570 (1985).
[18] H. de Waard, E. N. Kaufmann, and J. W. Rogers, Z. Phys. **264**, 423 (1973).
[19] D. M. Gordon, L. S. Eytel, H. de Waard, and D. E. Murnick, Phys. Rev. C **12**, 628 (1975).
[20] A. Arnesen, K. Johansson, E. Karlsson, T. Noreland, L.-O. Norlin, and S. Ogaza, Hyperfine Interact. **5**, 81 (1977).
[21] K.-H. Speidel, H. Busch, S. Kremeyer, U. Knopp, J. Cub, M. Bussas, W. Karle, K. Freitag, U. Grabowy, and J. Gerber, Nucl. Phys. **A552**, 140 (1993).
[22] Yu. V. Sergeenkov, Nucl. Data Sheets **58**, 765 (1989).
[23] Yu. V. Sergeenkov, Nucl. Data Sheets **65**, 277 (1992).
[24] Yu. V. Sergeenkov, Nucl. Data Sheets **71**, 557 (1994).
[25] J. K. Tuli, Nucl. Data Sheets **71**, 1 (1994).
[26] T. J. Mertzimekis, N. Benczer-Koller, J. Holden, G. Jakob, G. Kumbartzki, K.-H. Speidel, R. Ernst, A. Macchiavelli, M. McMahan, L. Phair, P. Maier-Komor, A. Pakou, S. Vincent, and W. Korten, Phys. Rev. C **64**, 024314 (2001).
[27] P. Maier-Komor, K.-H. Speidel, and A. Stolarz, Nucl. Instrum. Methods Phys. Res. A **334**, 191 (1993).
[28] J. F. Ziegler, J. Biersack, and U. Littmark, *The Stopping and Range of Ions in Solids* (Pergamon, Oxford, 1985), Vol. 1.
[29] O. Kenn, K.-H. Speidel, R. Ernst, J. Gerber, P. Maier-Komor, N. Benczer-Koller, G. Kumbartzki, and F. Becker, Nucl. Instrum. Methods Phys. Res. B **171**, 589 (2000).
[30] A. Piqué, J. M. Brennan, R. Darling, R. Tanczyn, D. Ballon, and N. Benczer-Koller, Nucl. Instrum. Methods Phys. Res. A **279**, 579 (1989).
[31] A. Winther and J. de Boer, *A Computer Program for Multiple Coulomb Excitation*, in *Coulomb Excitation*, edited by K. Alder and A. Winther (Academic, New York, 1966).
[32] R. Ernst, K.-H. Speidel, O. Kenn, A. Gohla, U. Nahum, J. Gerber, P. Maier-Komor, N. Benczer-Koller, G. Kumbartzki, G. Jakob, L. Zamick, and F. Nowacki, Phys. Rev. C **62**, 024305 (2000).
[33] J. C. Wells and N. R. Johnson, computer code LINESHAPE, ORNL, 1994.
[34] Ramendra Majumdar, Phys. Rev. C **55**, 745 (1997).
[35] G. Jakob, J. Cub, K.-H. Speidel, S. Kremeyer, H. Bisch, U. Grabowy, A. Gohla, O. Jessensky, and J. Gerber, Z. Phys. D: At., Mol. Clusters **32**, 7 (1994).
[36] B. H. Wildenthal, in *Understanding the Variety of Nuclear Excitations*, edited by A. Covello (World Scientific, Singapore, 1991), p. 35.
[37] A. Holt, T. Engeland, E. Osnes, M. Hjorth-Jensen, and J. Suhonen, Nucl. Phys. **A618**, 107 (1997).
[38] J. Blomqvist, Acta Phys. Pol. B **30**, 697 (1999).
[39] A. Holt, T. Engeland, M. Hjorth-Jensen, and E. Osnes, Nucl. Phys. **A634**, 41 (1998).
[40] G. N. White, N. J. Stone, J. Rikovska, S. Ohya, J. Copnell, T. J. Giles, Y. Koh, I. S. Towner, B. A. Brown, B. Fogelberg, L. Jacobsson, P. Rahkila, and M. Hjorth-Jensen, Nucl. Phys. **A644**, 277 (1998).
[41] S. Sarkar and M. S. Sarkar, Phys. Rev. C **64**, 014312 (2001).
[42] A. Etchegoyen, W. D. Rae, N. S. Godwin, W. A. Richter, C. H. Zimmerman, B. A. Brown, W. E. Ormand, and J. S. Winfield, computer code OXBASH, MSU-NSCL Report No. 524, 1985 (unpublished).
[43] A. Wolf and E. Cheifetz, Phys. Rev. Lett. **36**, 1072 (1976).
[44] B. Fogelberg, C. Stone, R. L. Gill, H. Mach, D. D. Warner, A. Aprahamian, and D. Rehfield, Nucl. Phys. **A451**, 104 (1986).
[45] J. Copnell, S. J. Robinson, J. Jolie, and K. Heyde, Phys. Rev. C **46**, 1301 (1992).